Nuclear Instruments and Methods in Physics Research A 840 (2016) 145–152

Contents lists available at ScienceDirect

Nuclear Instruments and Methods in Physics Research A

journal homepage: www.elsevier.com/locate/nima

4H-SiC Schottky diode arrays for X-ray detection

G. Lioliou[a,*], H.K. Chan[b], T. Gohil[a], K.V. Vassilevski[b], N.G. Wright[b], A.B. Horsfall[b], A.M. Barnett[a]

[a] Semiconductor Materials and Devices Laboratory, School of Engineering and Informatics, University of Sussex, Falmer, Brighton BN1 9QT, UK
[b] School of Electrical and Electronic Engineering, Newcastle University, Newcastle upon Tyne NE1 7RU, UK

ARTICLE INFO

Keywords:
Silicon carbide
Schottky diodes
X-ray spectroscopy
High temperature

ABSTRACT

Five SiC Schottky photodiodes for X-ray detection have been electrically characterized at room temperature. One representative diode was also electrically characterized over the temperature range 20°C to 140 °C. The performance at 30 °C of all five X-ray detectors, in both current mode and for photon counting X-ray spectroscopy was investigated. The diodes were fabricated in an array form such that they could be operated as either a 2×2 or 1×3 pixel array. Although the devices showed double barrier heights, high ideality factors and higher than expected leakage current at room temperature (12 nA/cm^2 at an internal electric field of 105 kV/cm), they operated as spectroscopic photon counting soft X-ray detectors uncooled at 30 °C. The measured energy resolution (*FWHM* at 17.4 keV, Mo Kα) varied from 1.36 to 1.68 keV among different diodes.

1. Introduction

Due to its wide bandgap [1] and good availability, silicon carbide has been studied for its suitability in high power and high temperature electron devices. In recent years it has also been considered for the development of photon counting X-ray spectroscopy in harsh environments. Its physical properties can lead to good performance at high temperatures and intense radiation environments; its large bandgap (2.3eV to 3.3 eV depending on the polytype [2], 3.27 eV for 4H-SiC) yields low thermally generated currents. Also, its relatively low electron affinity (=3.17 eV for 4H-SiC [3]) results in a high Schottky barrier and consequently in reduced thermionic emission current, minimizing the parallel white noise of the spectrometer system [4]. Noise due to charge trapping can also be minimized due to the short transit times for the charge carriers in SiC detectors as a result of its high breakdown field and high carrier saturation velocities [5].

The first experimental results with X-ray 4H-SiC Schottky detectors were reported in ref. [6], where X- and γ-ray spectra were obtained. Following this, rapid development of prototype single pixel spectroscopic systems using SiC epitaxial layers and ultralow noise electronics were pursued [7]. Bertuccio et al. reported a reduced *FWHM* at 5.9 keV of 196 eV at 30 °C which was increased to 233 eV at 5.9 keV at 100 °C [8]. Work has also been conducted to develop SiC Schottky diodes with thin (18 nm) Schottky contacts in order to improve quantum efficiencies at low X-ray energies; an energy resolution (*FWHM* at 22 keV) of 1.47 keV at room temperature has been reported for such a device [9], with photon counting spectroscopic measurements at temperatures up to 80 °C and after proton irradiation also presented [10] which shows promising results for their use in harsh environments. Another approach to increasing the low energy quantum efficiency of 4H-SiC X-ray detectors has also been demonstrated through vertical interdigitated Schottky contact photodiodes, which were originally developed for UV detection [11]. These devices have been demonstrated to capable of soft X-ray photon counting spectroscopy albeit with low energy resolution (3 keV *FWHM* at 5.9 keV) due to the large capacitance of the prototype devices [11]. However, so far, work on SiC X-ray detectors has concentrated on the development and characterisation of single pixel systems.

In this paper, we report fabrication of a 4H-SiC Schottky diode array in a combined 2×2 and 1×3 pixel configuration together with electrical characterisation and X-ray detection. Five diodes in total constitute the arrays, with two of the diodes being part of both arrays (further details can be found in Section 2. Device structure). The electrical characterisation includes measurements of forward and reverse bias dark currents and capacitances of the five diodes at room temperature. Only one of the diodes was characterized over a temperature range of 20°C to 140 °C. The photogenerated current of all diodes in the presence of X-ray photons from a Mo X-ray tube was recorded as a function of applied reverse bias demonstrating operation of the devices as current mode detectors. Each diode was then coupled to low noise front-end electronics, and their performance as spectroscopic X-ray detectors characterized.

2. Device structure

4H-SiC Schottky diodes (250 μm×250 μm) were fabricated from a

* Corresponding author.

http://dx.doi.org/10.1016/j.nima.2016.10.002
Received 8 February 2016; Received in revised form 5 August 2016; Accepted 1 October 2016
Available online 05 October 2016

commercial epitaxial wafer (Cree Inc.). The wafer had an n type 20 μm epitaxial layer, on a resistive n type 350 μm SiC substrate. The substrate had a diameter of 76.2 mm, a resistivity of 25 m Ω cm and an off axis surface orientation of 8.0°. After an RCA clean [12], oxidation at 1150 °C in dry oxygen followed to form the 25 nm thick passivation layer. A common NiSix Ohmic contact, at the rear of the array, was formed from 5 nm Ti and 100 nm Ni layers which were sintered at 1100 °C in vacuum. Windows were opened in this thermal oxide using buffered hydrofluoric acid prior to deposition of the Schottky contacts. The NiSi Schottky contacts on the active side of the array for each pixel were formed by depositing 3 nm of Ti and 12 nm of Ni using e-beam evaporation and then annealing the samples at 600 °C. The bond pads were formed by depositing a 200 nm thick Au layer on top of a 5 nm thick Cr adhesion layer.

The diodes were fabricated in a combined 2×2 and 1×3 array as per the mask layout is shown in Fig. 1. Four diodes constitute the 2×2 array and three constitute the 1×3 array. Due to the mask layout, two of the diodes are part of both arrays. The devices were mounted in a ceramic package and wire bonded.

3. Current–voltage measurements

Dark current measurements as a function of applied forward and reverse bias were performed using a Keithley 6487 Picoammeter/Voltage Source. The results are presented in Fig. 2.

As can be seen in Fig. 2(a), the shape of the forward current as a function of applied voltage of diode D3 is different compared to the rest of the devices. Diodes D1, D2, D4 and D5 exhibit double barrier heights, possibly as a result of excess pressure being applied to the contact during wire bonding.

The saturation current, I_s, was found from extrapolating the linear region of the dark current as a function of forward bias, to zero voltage. Using the values of the saturation current for each diode the zero band barrier height, φ_{OB}, was extracted and using the Cheung method [13], the ideality factor, n, was extracted from the dark current as a function of forward bias. Diode D3 was found to have the highest zero band barrier height (1.25 eV) whereas D5 had the lowest zero band barrier height (1.04 eV). An average zero band barrier height of (1.14 ± 0.07) eV (rms deviance) was found for all five diodes. This value is comparable with the zero band barrier height extracted for similar devices (1.21 eV) [10]. An average ideality factor of 2.1 ± 0.1 (rms deviance) was found for all diodes with diode D1 showing the lowest ideality factor (1.9). The variance of the ideality factor among the diodes was found to be within the uncertainty of the measurements (= ± 0.1). Although previous reports on similar devices showed ideality factors close to unity [10], the ideality factor values of the currently reported diodes suggest that the current mechanism is dominated by generation – recombination [14].

All the diodes were reverse biased up to −200 V, at 20 °C and showed leakage currents less than 70 pA (112 nA/cm^2) at −200 V reverse bias. Diode D4 exhibited the lowest reverse dark current at all applied reverse biases: 28 pA (44.8 nA/cm^2) at 170 kV/cm. Its current density was 13.9 nA/cm^2 (8.7 pA) at an internal electric field of 105 kV/cm, whereas a leakage current density of 1.6 nA/cm^2 (1 pA) has been previously reported for a similar device at the same electric field and at room temperature [10]. The leakage current mechanism, resulting in unexpected high leakage current densities at room temperature is discussed below. The presently reported detectors have much higher room temperature leakage currents than the lowest reported in the literature for SiC detectors (1 pA/cm^2 [8] at 103 kV/cm) and commercial 4H-SiC Schottky diodes (347 pA/cm^2 at 403 kV/cm [15]).

To characterize the performance of the detectors with temperature, one of the diodes, D3, was installed inside a TAS Micro MT climatic cabinet and its forward and reverse dark currents measured over the temperature range 20°C to 140 °C. Diode D3 was selected due to the absence of a double barrier height and its leakage current being the lowest compared to the rest of the diodes. Fig. 3 shows the temperature dependent dark current as a function of applied bias of this diode.

For applied forward bias up to 1.35 V, the measured current increased with increased temperature due to recombination current being the main current generation mechanism, which is proportional to the intrinsic carrier concentration, n_i. However, a different behaviour observed at higher current values and at forward applied biases greater than 1.35 V. Optical phonon scattering resulted in the reduction of the electron mobility which influenced the electrical behaviour at high current values region [16].

The ideality factor, n, and the zero band barrier height, φ_{OB}, were extracted for diode D3 over the temperature range 20°C to 140 °C following the same procedure as described above. The results are presented in Fig. 4. The ideality factor improved from 1.99 at 20 °C to 1.81 at 140 °C and the zero band barrier height increased from 1.32 eV at 20°C to 1.49 eV at 140 °C. The improvement of the ideality factor and the increase in the zero band barrier height as the temperature increased can be explained by the presence of an inhomogeneous barrier [17,18]. The current through an inhomogeneous barrier can be expressed as the sum of currents flowing in lower Schottky barrier height patches [18]. The low apparent Schottky barrier height (1.32 eV) at 20 °C was attributed to the current being dominated by electrons surmounting the lower barriers. As the temperature increased, electrons had more energy to overcome higher barriers resulting in a higher zero band barrier height and improved ideality factor.

As expected, the leakage current was found to increase with increased temperature at all investigated reverse biases. Fig. 5 shows the measured leakage current as a function of temperature at −200 V and −80 V reverse bias. The current exponentially increased at temperatures above 100 °C, which was consistent with Schottky-barrier lowering [14]. However, within the temperature range 20°C to 80 °C, the dominant mechanism of the measured leakage current was different compared to that at higher temperatures.

To further investigate the leakage current mechanism at different temperatures, the activation energy, E_a, was extracted from the Arrhenius plot. For the temperature range where the activation energy was constant the ln(I) as a function of $1/T$ graph, shown in Fig. 6,

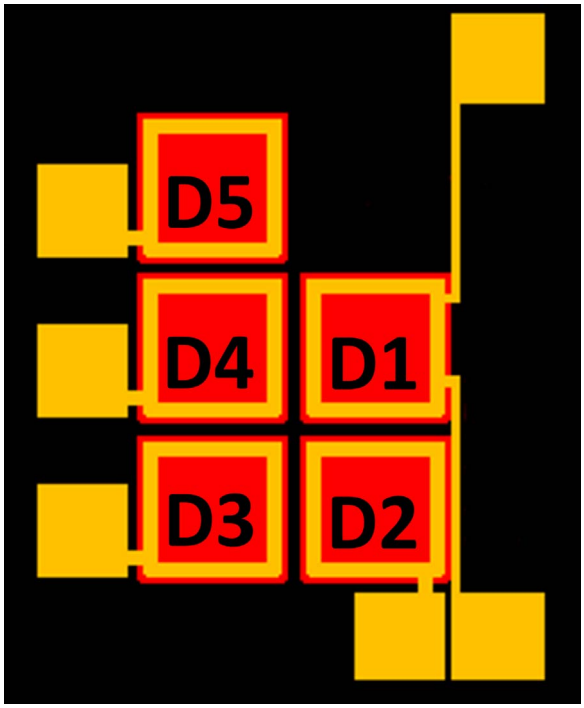

Fig. 1. Mask layout showing the combined 2×2 and 1×3 array.

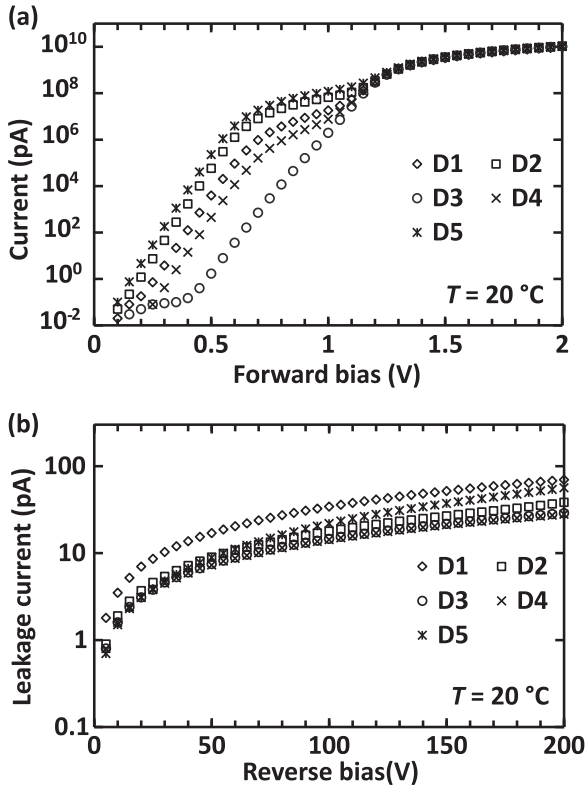

Fig. 2. Leakage current measured at a temperature of 20 °C for the five SiC Schottky photodiodes, D1 – D5, as a function of (a) forward and (b) reverse bias. D1 – open diamonds; D2 – open squares; D3 – open circles; D4 – × symbols; D5 – stars.

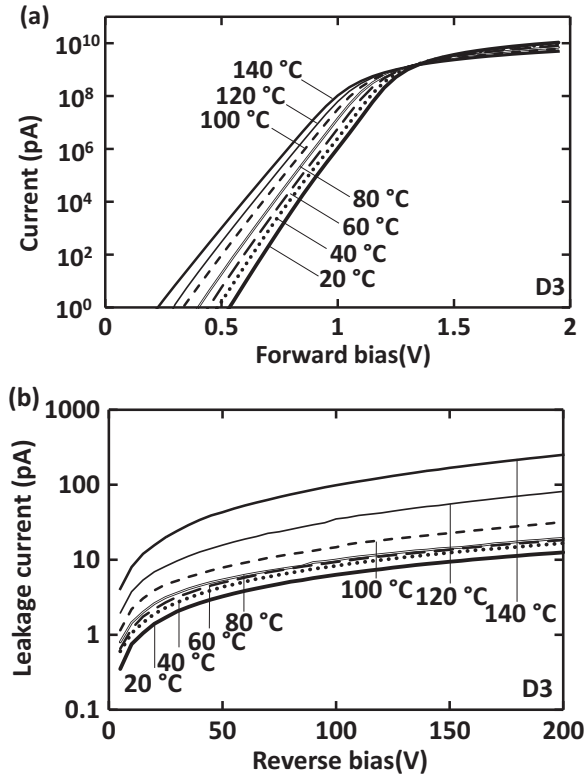

Fig. 3. Measured dark current as a function of (a) forward and (b) reverse bias at a temperature range of 20–140 °C, for diode D3. 140 °C – square dots; 120 °C – thin solid line; 100 °C – dashes; 80 °C – long dash dot; 60 °C – long dashes; 40 °C – big round dots; 20 °C – thick solid line.

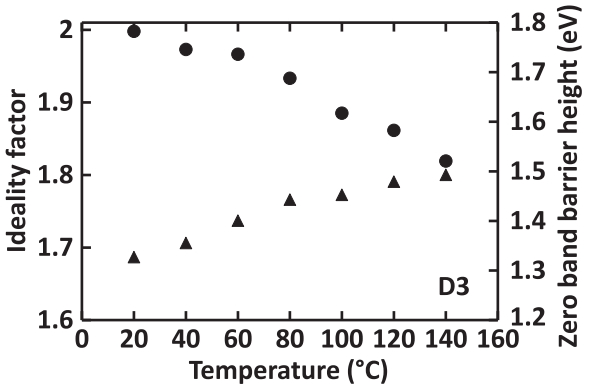

Fig. 4. Ideality factor (circles) and zero band barrier height (triangles) extracted from forward current – voltage graph in the temperature range 20–140 °C for D3.

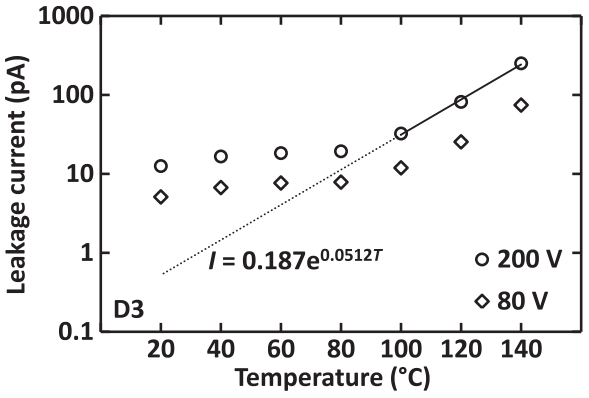

Fig. 5. Leakage current as a function of temperature at −200 V (circles) and −80 V (diamonds) reverse bias for D3. The line of best fit calculated using linear least squares fitting for the temperature range 100°C to 140 °C and 200 V reverse bias is also shown (solid line) along with the extrapolated line for the temperature range 20°C to 100 °C (dots).

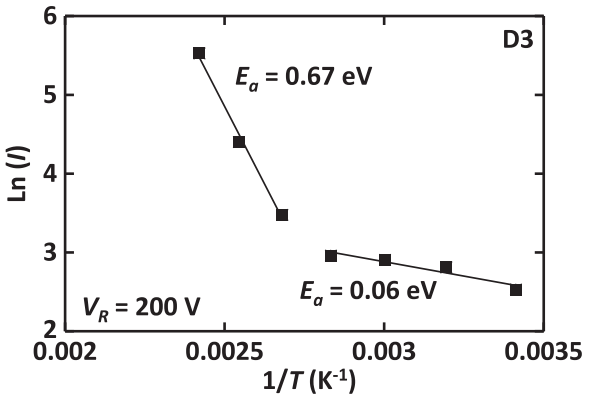

Fig. 6. Arrhenius plot to extract the activation energy for D3.

yielded a straight line [5]. The gradient of this line was used to calculate the activation energy

$$\ln(I)=\ln(AT^2)-\frac{E_a}{kT}. \quad (1)$$

Two linear regions can be seen in Fig. 6. The activation energy was found to be ~0.06 eV in the temperature range 20°C to 80 °C and ~0.67 eV in the temperature range 100°C to 140 °C. The energy level at low temperatures was associated with nitrogen (*n*-type epilayer dopant) carrier generation with ionization energy of 0.052 eV in 4H-SiC [19]. When SiC is doped with nitrogen, various complexes may be formed in association with intrinsic defects of the SiC or background impurities. A donor level of 0.6 eV, similarly to the activation energy

found at high temperatures, has been reported for Ti-N pairs in 4H-SiC having different position in the lattice compared to a single nitrogen atom. The low activation energy at low temperatures (=0.06 eV), indicates a weak dependency of leakage current on temperature. At high temperatures, the leakage current of diode D3 was comparable with a previously reported similar device [10]. As an example, both the currently reported device, D3 and the device reported in ref. [10] had a leakage current < 10 pA at −80 V reverse bias and 80 °C. However, the leakage current of D3 only slightly decreased from 8 pA at 80 °C to 5 pA at 20 °C, both at −80 V reverse bias.

4. Capacitance–voltage measurements

The depletion width, the effective carrier concentration, and the flat band barrier height of the diodes were determined from capacitance measurements. The capacitance of the diodes was measured as a function of applied forward and reverse bias using an HP 4275 A Multi frequency LCR meter. The test signal was sinusoidal with a 50 mV rms magnitude and 1 MHz frequency. The measured capacitance consisted of the device (depletion-layer) capacitance, C_D, and the capacitance of the package, C_{pack}. Due to the nature of the packaging, each diode had a difference C_{pack}. An estimation of each C_{pack} was made based on capacitance measurements of empty pins of the package. Fig. 7 shows the measured capacitance (C_{pack} subtracted) of all five diodes at a temperature of 20 °C.

At 0 V applied bias and 20 °C, comparable capacitances were recorder for four devices (D2–D5), with a mean value of 5.83 pF ± 0.22 pF. Diode D1 showed a higher capacitance (8.05 pF). As the applied reverse bias, V_a, increased, the capacitance, C_D, was found to decrease as expected. More specifically, as the reverse bias increased from 0 V to −50 V, the capacitance of four diodes (D2–D5) decreased by 4.87 pF ± 0.09pF to 0.96 pF ± 0.15 pF, whereas the other diode, D1, showed a larger decrease of 7.05pF to 1.00 pF. As the reverse bias was further increased in magnitude from −50 V to −100 V, there was an additional reduction in capacitance of 0.30 pF ± 0.04 pF for all diodes. For all diodes, a 0.23 pF ± 0.04 pF reduction in capacitance was recorded as the reverse voltage increased in magnitude from −100 V to −200 V. The depletion width, W_D, was calculated based on the measured depletion-layer capacitance, C_D,

$$W_D = \frac{\varepsilon \varepsilon_0 A}{C_D} \tag{2}$$

where ε (=9.66 [20]) is the dielectric constant of SiC, ε_O is the permittivity of free space and A is the area of the diode [14]. The calculated depletion width of each diode as a function of applied reverse bias can be seen in Fig. 8. Additionally, the calculated quantum efficiency, QE, of the detectors at 17.4 keV X-ray energy as a function of applied reverse bias assuming 3 nm Ti and 12 nm Ni dead layers and only the depletion layer width being the active layer can be seen in Fig. 8.

The depletion widths of the diodes were found to range from 10 μm to 14 μm at −200 V reverse bias. The variation in the depletion width of the diodes was attributed to the uncertainty of the capacitance of the package, C_{pack}. The different capacitance change, ΔC, as the voltage increased from 0 V to −200 V reverse bias among the diodes suggested that possible variations on the doping concentration at the epilayer across the wafer could also contribute to the variation in the depletion width of the diodes as seen in Fig. 8.

The effective carrier concentration, N_{eff}, and the flat band barrier height, φ_{FB}, were computed at 20 °C from C^{-2} as a function of applied voltage, V_a, for one representative diode, D3 (see Fig. 9).

The effective carrier concentration, N_{eff}, was computed by

$$N_{eff} = \frac{2}{q\varepsilon\varepsilon_0 A^2}\left[-\frac{1}{d(1/C_D^2)/dV_a}\right], \tag{3}$$

where $d(1/C^2)/dV$ is the gradient of the line of best fit [14]. The effective carrier concentration was found to be 16.7×10^{14} cm^{-3}. The flat band barrier height, φ_{FB}, for diode D3 at 20 °C, which was computed using the intercept point on the voltage axis V_i as follows,

$$\varphi_{FB} = V_n + V_{bi} = \frac{kT}{q}\ln\left(\frac{N_c}{N_D}\right) + V_i + \frac{kT}{q}, \tag{4}$$

where N_c is the effective density of states in the conduction band of SiC (1.5×10^{25} m^{-3} at room temperature based on the electron effective masses [21]) [14], was found to be φ_{FB} =1.48 eV and the built in voltage, V_{bi} =1.26 V (corresponding to a value of V_i =1.24 V).

To investigate the capacitance characteristics of the devices at elevated temperatures, the same diode as it was used for the temperature dependent current measurements, D3, was placed inside a TAS Micro MT climatic cabinet. The diode's capacitance at both forward and reverse biases was measured over the temperature range 20–140 °C. Fig. 10 shows the temperature dependent capacitance as a function of applied bias of diode D3.

At each applied forward bias, the capacitance of D3 was measured to be greater at higher temperatures over the temperature range 20–140 °C (Fig. 10a). At each applied reverse bias the capacitance of D3 was measured to be greater at higher temperatures over the temperature range 80°C to 140 °C (Fig. 10b). This small increase of the capacitance was attributed to the increase of the charge density at the depletion layer as the temperature increased due to the presence of deep centers whose occupancy was temperature dependent, similarly to ref. [22]. Over the temperature range 20°C to 80 °C, the capacitances measured at each applied bias were similar (Fig. 10b).

5. X-ray detection measurements

All five diodes were installed within a LD Didactic GmbH X-ray apparatus having a Mo target X-ray tube. The temperature inside the apparatus cabinet was 30 °C. The diodes were characterized for their

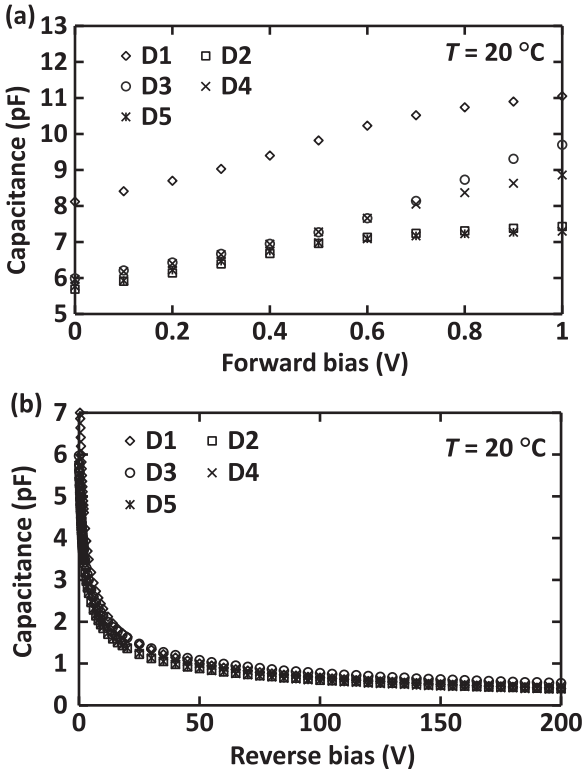

Fig. 7. Measured capacitance as a function of (a) forward and (b) reverse bias at a temperature of 20 °C for the five SiC Schottky photodiodes, D1–D5. D1 – open diamonds; D2 – open squares; D3 – open circles; D4 – × symbols; D5 – stars.

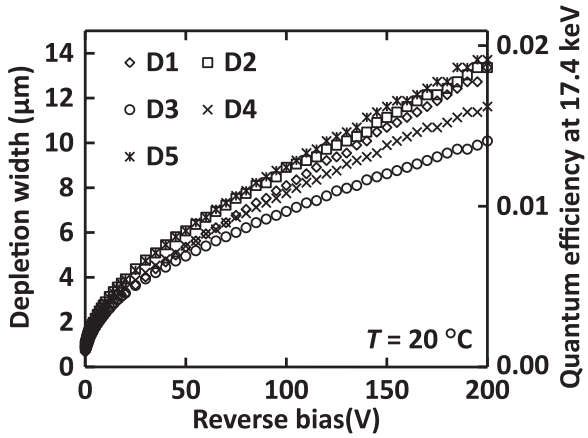

Fig. 8. Calculated depletion width (left y-axis) and quantum efficiency at 17.4 keV (right y-axis) for the five SiC Schottky photodiodes, D1–D5, as a function of reverse bias at a temperature of 20 °C. D1 – open diamonds; D2 – open squares; D3 – open circles; D4 – × symbols; D5 – stars.

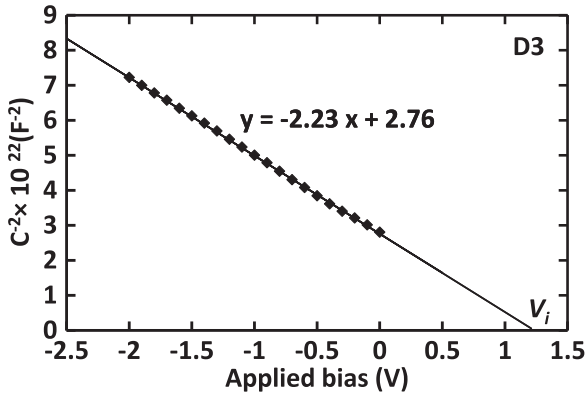

Fig. 9. C^{-2} plot as a function of applied voltage, V, for diode D3 at a temperature of 20 °C. The line of best fit as determined by linear least squares fitting is also shown.

response to X-ray illumination. Each diode was positioned inside a custom test fixture with a 4 μm Al window, directly in-line with aperture to the X-ray tube. The leakage current of each diode was measured as a function of applied reverse bias. Then, the X-ray tube, with its voltage and current being 35 kV and 1 mA respectively, was switched on. The total current (dark plus photocurrent) was recorded as a function of applied reverse bias for each diode. Fig. 11 shows the measured dark and illuminated currents for diode D5 at 0 V to −200 V reverse bias.

The leakage current was subtracted from the total current, to give the photogenerated current which can be seen for each of the five diodes as a function of reverse bias in Fig. 12. The photocurrent was measured to range from 4 pA to 8 pA for all diodes at reverse biases up to −100 V.

Following the photocurrent measurements, X-ray spectra were obtained using all the diodes. Each diode was connected in turn to a single channel custom-made charge sensitive preamplifier of feedback resistorless design similar to that described in Ref. [23]. Both the diode and the preamplifier were housed in a custom test fixture with a 4 μm Al window, which was positioned inside the X-ray apparatus in-line with the X-ray tube aperture. The output signal of the preamplifier was shaped using an Ortec 572 A shaping amplifier. The output of the shaping amplifier was connected to a multi-channel analyzer (MCA) for digitization. The live time of each accumulate spectrum was 300 s.

Spectra were obtained using D5 at different shaping times (τ=0.5 μs, 1 μs, 2 μs, 3 μs, 6 μs and 10 μs), with the diode being reverse biased at −60 V. Gaussians were fitted to the detected Mo Kα (=17.4 keV) and Kβ (=19.6 keV) peaks of the accumulated spectra,

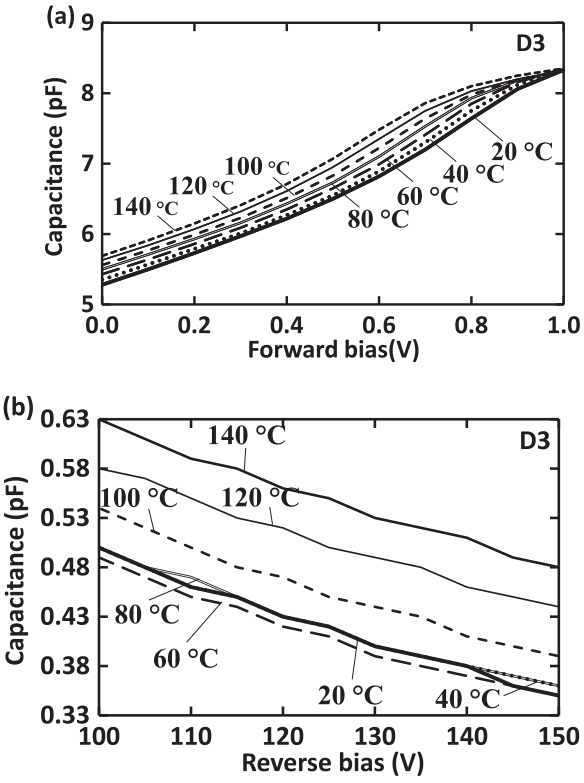

Fig. 10. Measured capacitance as a function of (a) forward and (b) reverse bias at a temperature range of 20–140 °C, for diode D3; 140 °C – square dots; 120 °C – thin solid line; 100 °C – dashes; 80 °C – long dash dot; 60 °C – long dashes; 40 °C – large round dots; 20 °C – thick solid line.

while the position of the zero energy noise peak and the Mo Kα peak were used to energy calibrate each spectrum. The measured *FWHM* at 17.4 keV as a function of shaping time with D5 (reverse biased at −60 V) can be seen in Fig. 13.

The energy resolution (*FWHM* at 17.4 keV) at the optimum shaping time (τ_{opt} =1 μs) was found to be 1.43 keV. Spectra of the Mo X-ray tube were then subsequently obtained using the other diodes operated at 1 μs shaping time. The diodes were kept reverse biased at −60 V. An average depletion layer width of 6.1 μm ± 0.5 μm (rms deviance) was found for all diodes at -60 V reverse bias (Fig. 8). The variance of depletion width among the diodes was found to be within the uncertainty of the measurements at -60 V (= ± 2 μm). A quantum efficiency of 0.85% at 17.4 keV was calculated for all diodes (Fig. 8). The best energy resolution was achieved with diode D4 (*FWHM* at 17.4 keV=1.36 keV), whereas the poorest energy resolution was found to be 1.68 keV using diode D1, which had the highest leakage current

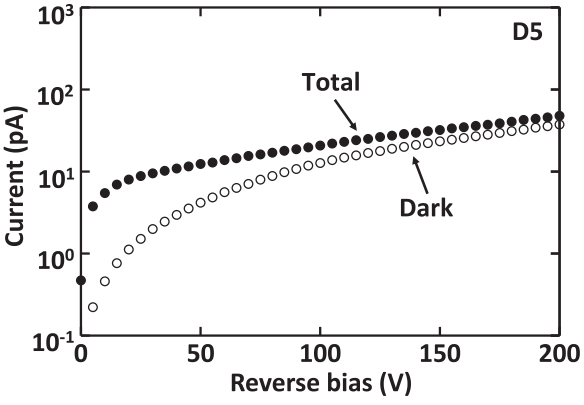

Fig. 11. Measured current of diode D5 as a function of reverse bias for X-ray tube being off (dark current) and on (total current).

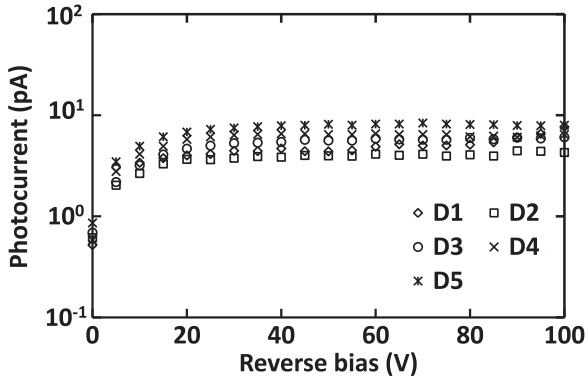

Fig. 12. Measured photogenerated current as a function of reverse bias from X-ray photons, of all diodes; D1 – open diamonds; D2 – open squares; D3 – open circles; D4 – × symbols; D5 – stars.

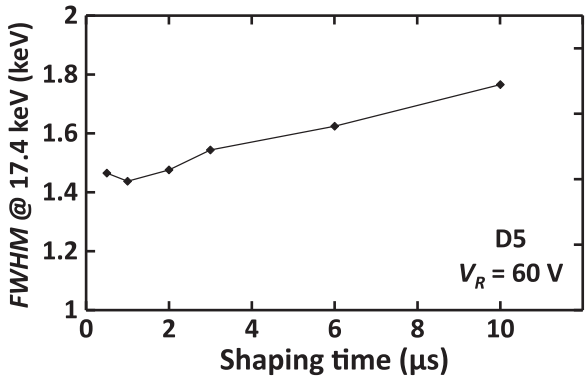

Fig. 13. Energy resolution (*FWHM* at 17.4 keV) as a function of shaping time for diode D5 when reverse biased at 60 V. Line is only a guide to the eye.

(20.4 pA, see Fig. 2) and capacitance (2.2 pF, including the packaging capacitance) at −60 V reverse bias. The spectrum of the Mo target X-ray tube obtained using all five diodes, D1-D5, at 1 μs and −60 V reverse bias can be seen in Fig. 14.

The leakage currents of the detector and preamplifier's input JFET of the give rise to the parallel white noise. The capacitance of the detector and of the input JFET of the preamplifier give rise to the series white noise. Each component of the electronic noise (parallel white noise, series white noise, $1/f$ noise) was calculated as described in ref. [24]. The Fano noise was calculated to be equivalent to a *FWHM* of 274 eV at 17.4 keV, assuming F=0.1 and ω=7.8 eV. By subtracting the expected Fano noise, along with the calculated white series, white parallel, and $1/f$ noise contributions in quadrature from the determined energy resolution as quantified by the *FWHM*, the remaining was attributed to stray capacitances (unknown white series noise) and dielectrics (dielectric noise) in close proximity to the input of the preamplifier. The total noise along with the calculated contributions for each different noise source can be seen in Fig. 15 for each of the diodes.

The analysis presented in Fig. 15 indicates that the noise arising from stray capacitances and dielectrics at the input of the preamplifier was the dominant source of noise in the reported system; (1.34 ± 0.11) keV (equivalent to (73 ± 6) e^- rms) *FWHM* at 17.4 keV. This result is comparable with similar previously reported preamplifier systems, which have a dielectric noise of 70 e^- rms [25] and 72 e^- rms [26]. Due to the pinout of the package of the devices, the connection of each device to the preamplifier was different resulting in a different unknown stray capacitance for each diode. Consequently, the unknown white series noise varied among the diodes as it was the dielectric noise, with the latter being dependent on the total capacitance at the input of the preamplifier. The charge trapping noise was assumed to be negligible at −60 V reverse bias due to improved charge transport at electric field strengths of ~100 kV/cm compared to lower electric fields. However, the presence of the charge trapping noise cannot be directly measured. Hence, the charge trapping noise can be included in the sum of the unknown noise components: the unknown series white noise and dielectric noise.

The *FWHM* at 17.4 keV ranged from 1.36 keV (D4) to 1.68 keV (D1), at 30 °C. These results are comparable with previously reported semi-transparent SiC Schottky diodes (1.49 keV at 5.9 keV at 23 °C [9] and 1.36 keV at 22.16 keV [10]) and better than commercial 4H-SiC Schottky diodes (1.8 keV at 5.9 keV [15]) connected to similar preamplifier systems. However, they are not as good as the best experimental reports on single pixel SiC X-ray detectors (196 eV *FWHM* at 5.9 keV at 30 °C [8]); which were achieved using 4H-SiC epitaxial layers of exceptional quality and ultra low noise electronics. It should be noted that compared to systems employing detectors made from silicon or materials with narrow bandgaps, the electronic noise of the preamplifier used with a wide bandgap semiconductor detector, such as SiC, is more critical due to the typically greater electron hole pair creation energy of wide bandgap materials (7.8 eV for SiC [4] as opposed to 3.6 eV for Si [27]). For example, a total equivalent noise charge of 70 e^- rms (excluding Fano noise) at the input of a preamplifier results in a *FWHM* of 600 eV when a Si detector is used, and 1300 eV when a SiC detector is used.

6. Discussions, conclusions and future work

A 2×2 and a 1×3 SiC diode array, consisting of five diodes in total, have been electrically characterized at room temperature. In addition, one representative diode was characterized at elevated temperatures (up to 140 °C). Use of diodes as X-ray detectors in both current mode and spectroscopic X-ray photon counting mode has been demonstrated for all diodes at a temperature of 30 °C.

The forward current characteristics suggested that four diodes (D1 – D2 and D4 – D5) had a double barrier height. The extracted zero band barrier height was found to be 1.14 eV ± 0.07 eV (rms deviance). The ideality factor (=2.1 ± 0.1) deviated from unity, indicating that, at room temperature, the main current mechanism was not thermionic emission. All the diodes were reverse biased at up to −200 V (~160 kV/cm) and had leakage currents under 70 pA at −200 V reverse bias and at room temperature.

Forward and reverse bias current measurements on D3 at elevated temperatures (up to 140 °C) revealed the possible presence of an inhomogeneous barrier. Over the investigated temperature range, the ideality factor of D3 improved from 1.99 at 20 °C to 1.81 at 140 °C, and the zero band barrier height increased from 1.32 to 1.49 at the same temperatures. It was also found that at the temperature range 20°C to 80 °C the leakage current did not follow the expected temperature dependence, this was attributed to the leakage current originating from surface components around the contact. The double barrier height, the high ideality factor, and the high leakage current at room temperature are consistent with damage from suboptimal wire bonding.

Comparable capacitances (=5.83 pF ± 0.22 pF at 0 V) were measured for four of the devices, D2–D5, at both forward and reverse biases, but one device, D1 showed a moderately higher capacitance at 0 V (=8.05 pF) and at forward biases. The depletion width was found to range from 10 μm to 14 μm among the diodes at the highest investigated reverse bias (−200 V), however this was mostly attributed to the uncertainty of each packaging capacitance. The effective carrier concentration and flat band barrier height at room temperature was calculated for one representative diode, D3, and were found to be 16.7×10^{14} cm^{-3} and 1.49 eV respectively. The temperature dependence of the same diode's capacitance was also measured. It was found that its capacitance slightly decreased as the temperature decreased from 5.7 pF at 140°C to 5.5 pF at 80 °C, at 0 V, due to possible effective charge density decrease related to the occupancy of deep level defects.

The X-ray response of the diodes as a function of reverse bias was

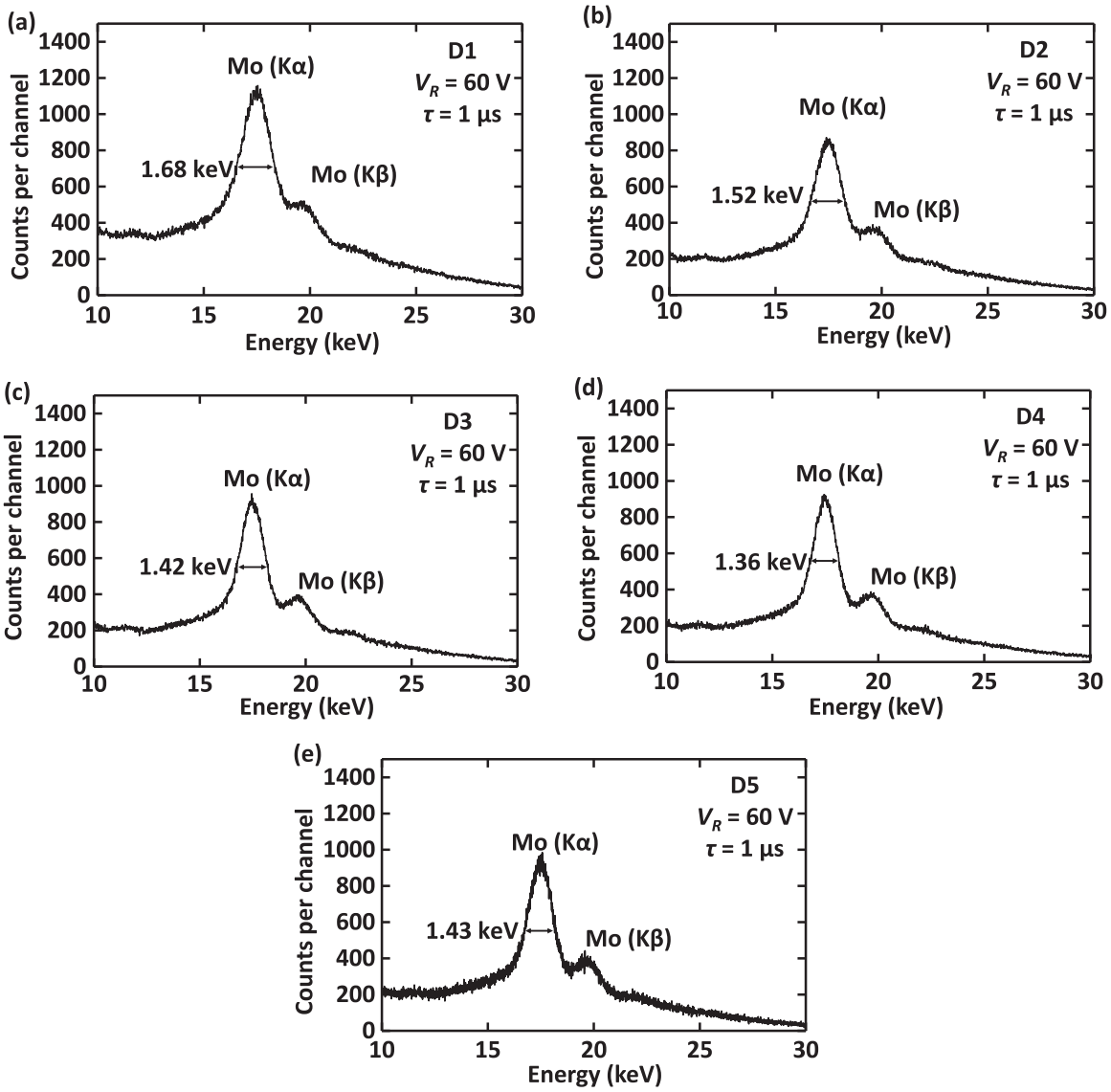

Fig. 14. Spectra of the Mo target X-ray tube accumulated with photodiode a) D1, b) D2, c) D3, d) D4 and e) D5 at 1 μs shaping time and −60 V reverse bias.

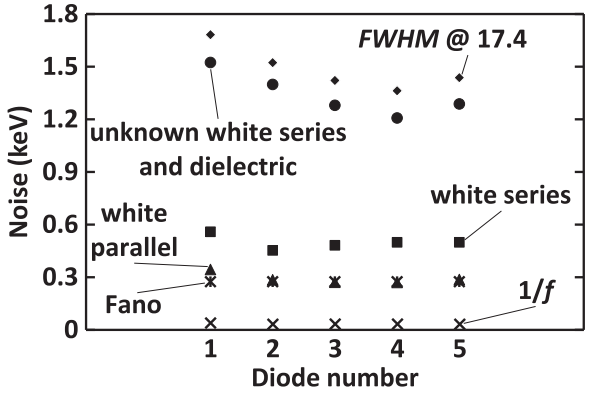

Fig. 15. The calculated noise contributions for all five SiC diodes, at 1 μs shaping time and 60 V reverse bias. 1/*f* noise (crosses), parallel white noise (filled triangles), Fano noise (stars), known series white noise (filled squares), sum of unknown white series noise and dielectric noise (filled circles) and total noise (energy resolution as quantified by the *FWHM* at 17.4 keV) (filled diamonds).

studied by measuring the photogenerated current in the devices when they were illuminated with a Mo X-ray tube. All five diodes were sensitive to X-rays and showed comparable photogenerated currents in the range of 4 pA to 8 pA at −100 V reverse bias.

To evaluate the devices for photon counting X-ray spectroscopy, the diodes were coupled to a custom made low noise charge sensitive preamplifier. Spectra were obtained using the same Mo X-ray tube as was used for the current mode X-ray measurements. The *FWHM* of the Mo Kα peak was measured; using diode D5, it was found that the optimum shaping time was 1 μs. The diodes were reverse biased at −60 V and the energy resolution (*FWHM* at 17.4 keV) achievable with each diode was measured; it ranged from 1.36 keV (D4) to 1.68 keV (D1), at ~30 °C and 1 μs shaping time. The energy resolution of the system was found to be limited by the noise arising from the dielectric noise and stray capacitances present at the proximity of the preamplifier's input.

Although the pixels of the 2×2 and 1×3 SiC diode arrays reported here showed unexpected high leakage current at room temperature, double barrier heights and high ideality factors, we have shown that they can operate as detectors for photon counting X-ray spectroscopy at 30 °C with modest energy resolution. The importance of developing the electronics to which the detectors were connected was highlighted and work to reduce the dielectric noise through redesign of the preamplifier frontend will be reported in future publications.

Authors' data statement

Data underlying this work are subject to commercially confidentiality. The Authors regret that they cannot grant public requests for further access to any data produced during the study, however the key findings are fully included within the article.

Acknowledgements

In part, this work was supported by STFC, United Kingdom Grants ST/M002772/1 and ST/M004635/1 and Royal Society, United Kingdom Grant RS130515. G. Lioliou acknowledge funding received from University of Sussex in the form of a Ph.D. scholarship.

References

[1] F. Nava, G. Bertuccio, A. Cavallini, E. Vittone, Meas. Sci. Technol. 19 (2008) 102001.
[2] G.L. Harris, Prop. SiC. Inst. Electr. Eng. Lond. (1995).
[3] S. Yu Davydov, Semiconductors 41 (2007) 696.
[4] G. Bertuccio, R. Casiraghi, IEEE Trans. Nucl. Sci. 50 (2003) 175.
[5] G. Bertuccio, D. Puglisi, A. Pullia, C. Lanziery, IEEE Trans. Nucl. Sci. 60 (2013) 1437.
[6] G. Bertuccio, R. Casiraghi, F. Nava, IEEE Trans. Nucl. Sci. 48 (2001) 232.
[7] G. Bertuccio, R. Casiraghi, A. Cetronio, C. Lanziery, F. Nava, Nucl. Instrum. Methods Phys. Res. Sect. A 522 (2004) 413.
[8] G. Bertuccio, S. Caccia, D. Puglisi, D. Macera, Nucl. Instrum. Methods Phys. Res. Sect. A 652 (2011) 193.
[9] J.E. Lees, D.J. Bassford, G.W. Fraser, A.B. Horsfall, K.V. Vassilevski, N.G. Wright, A. Owens, Nucl. Instrum. Methods Phys. Res. Sect. A 578 (2007) 226.
[10] J.E. Lees, A.M. Barnett, D.J. Bassford, R.C. Stevens, A.B. Horsfall, J. Instrum. 6 (2011) C01032.
[11] J.E. Lees, A.M. Barnett, D.J. Bassford, M. Mazzillo, J. Instrum. 7 (2012) P11024.
[12] W. Kern, D.A. Puotinen, RCA Rev. 31 (1970) 187.
[13] S.K. Cheung, N.W. Cheung, Appl. Phys. Lett. 49 (1986) 85.
[14] S.M. Sze, Physics of Semiconductor Devices, 3rd ed., John Wiley & Sons, New Jersey, 2007.
[15] S. Zhao, T. Gohil, G. Lioliou, A.M. Barnett, Nucl. Instrum. Methods Phys. Res. Sect. A 830 (2016) 1.
[16] F. La Via, G. Galvagno, F. Roccaforte, A. Ruggiero, L. Calcagno, Appl. Phys. Lett. 87 (2005) 142105.
[17] F. Roccaforte, F. La Via, V. Raineri, R. Pierobon, E. Zanoni, J. Appl. Phys. 93 (2003) 9137.
[18] R.T. Tung, Appl. Phys. Lett. 58 (1991) 2821.
[19] A.A. Lebedev, Semiconductors 33 (1999) 107.
[20] L. Patrick, W.J. Choyke, Phys. Rev. B 2 (1970) 2255.
[21] N.T. Son, W.M. Chen, O. Kordina, A.O. Konstantinov, B. Monemar, E. Janzén, D.M. Hofman, D. Volm, M. Drechsler, B.K. Meyer, Appl. Phys. Lett. 66 (1995) 1074.
[22] G. Gramberg, Solid-State Electron. 14 (1971) 1067.
[23] G. Bertuccio, P. Rehak, D. Xi, Nucl. Instrum. Methods Phys. Res. Sect. A 326 (1993) 71.
[24] G. Lioliou, A.M. Barnett, Nucl. Instrum. Methods Phys. Res. Sect. A 801 (2015) 63.
[25] A.M. Barnett, J.E. Lees, D.J. Bassford, J.S. Ng, Nucl. Instrum. Methods Phys. Res. Sect. A 673 (2012) 10.
[26] G. Lioliou, X. Meng, J.S. Ng, A.M. Barnett, Characterization of Gallium Arsenide X-ray mesa p-i-n photodiodes at room temperature, Nucl. Instrum. and Methods Phys. Res. Sect. A 813 (2016) 1 (in preparation).
[27] G.W. Fraser, A.F. Abbey, A. Holland, K. McCarthy, A. Owens, A. Wells, Nucl. Instrum. Methods Phys. Res. Sect. A 350 (1994) 368.